



Palladium(0) nanoparticles supported on polydopamine coated CoFe_2O_4 as highly active, magnetically isolable and reusable catalyst for hydrogen generation from the hydrolysis of ammonia borane

Joydev Manna, Serdar Akbayrak, Saim Özkar*

Department of Chemistry, Middle East Technical University, 06800 Ankara, Turkey

ARTICLE INFO

Article history:

Received 29 December 2016
Received in revised form 4 February 2017
Accepted 10 February 2017
Available online 20 February 2017

Keywords:

Palladium nanoparticles
Cobalt ferrite
Polydopamine
Ammonia borane
Hydrogen
Catalysis

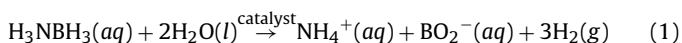
ABSTRACT

Palladium(0) nanoparticles supported on cobalt ferrite ($\text{Pd}^0/\text{CoFe}_2\text{O}_4$) are found to be highly active catalyst, providing an unprecedented catalytic activity with a turnover frequency of 290 min^{-1} in hydrogen generation from the hydrolysis of ammonia borane at room temperature. However, the initial catalytic activity of $\text{Pd}^0/\text{CoFe}_2\text{O}_4$ catalyst is not preserved after the reuse of the catalyst in hydrolytic dehydrogenation of ammonia borane. The stability of the catalyst is improved by using the polydopamine (PDA) coated cobalt ferrite as support instead of bare cobalt ferrite. PDA coating of CoFe_2O_4 nanopowders was achieved by pH-induced self-polymerization of dopamine hydrochloride at room temperature and the thickness of PDA was optimized by changing the amount of dopamine hydrochloride. Palladium(0) nanoparticles supported on PDA coated cobalt ferrite ($\text{Pd}^0/\text{PDA-}\text{CoFe}_2\text{O}_4$) were prepared by two step impregnation-reduction process and characterized by a combination of advanced analytical techniques. The results reveal that palladium nanoparticles with an average size of $1.4 \pm 0.3 \text{ nm}$ are well dispersed on polydopamine layer with a thickness of $8.6 \pm 1.0 \text{ nm}$ on the surface of cobalt ferrite nanopowders. $\text{Pd}^0/\text{PDA-}\text{CoFe}_2\text{O}_4$ with a palladium loading of 1.08 wt% was found to be a highly active and reusable catalyst in hydrogen generation from the hydrolysis of ammonia borane with a turnover frequency of 175 min^{-1} at $25.0 \pm 0.1 \text{ }^\circ\text{C}$. Magnetically isolable $\text{Pd}^0/\text{PDA-}\text{CoFe}_2\text{O}_4$ catalyst preserves its initial catalytic activity even after the tenth use providing the release of 3 equivalent H_2 per mole of ammonia borane.

© 2017 Elsevier B.V. All rights reserved.

1. Introduction

Ammonia borane (NH_3BH_3 , AB) is considered as one of the promising chemical hydrogen storage materials owing to its high hydrogen content (19.6 wt%), stability and non-toxicity [1,2]. Hydrolysis of ammonia borane is a widely accepted and well-studied method for hydrogen generation as it can release 3 mol H_2 per mole of NH_3BH_3 at ambient temperature in the presence of a suitable catalyst (Eq. (1)). Although a recent report has shown that the only byproduct of hydrolysis, ammonium metaborate, can be converted to ammonia borane [3], an efficient process is still needed for the regeneration of ammonia borane.



Several zero-valent transition metal nanoparticles of Pt [4,5], Pd [6,7], Ru [8,9], Rh [10,11], Ag [12,13], Co [14,15], Ni [16,17],

Fe [18,19], etc. have been shown to be catalytically active in hydrogen generation from the hydrolysis of AB. However, metal nanoparticles have tendency to aggregate to larger particles, ultimately to bulk metal and, therefore, they suffer in long-term stability. Metal nanoparticles can be stabilized against agglomeration by supporting materials with large surface area. Selecting a suitable support is crucial in obtaining stable and catalytically active metal nanoparticles with controllable size and size distribution [20,21]. So far, various supporting materials (metal oxides, zeolites, carbons, etc.) have widely been used to stabilize metal nanoparticles [22,23]. However, separation of these catalysts by filtration or centrifugation is one of the major problems in recycling the catalysts. Magnetic supports have recently attracted great interest in liquid phase catalytic reactions as they provide easy magnetic separation of nanoparticles [24], which is promising option for a catalyst to be used in practical applications with high accessibility and reusability [25]. Magnetite (Fe_3O_4) [26], maghemite ($\gamma\text{-Fe}_2\text{O}_3$) [27], and spinel ferrites (MFe_2O_4 M = Co, Ni, Zn, etc.) [28] are widely used as magnetic support materials in several organic and inorganic reactions. The active catalysts are

* Corresponding author.

E-mail address: sozkar@metu.edu.tr (S. Özkar).

supported either on the bare surface of magnetic particles or a coating layer such as silica, carbon or polymer on magnetic particles. Among the magnetic supporting materials, cobalt ferrite (CoFe_2O_4) has attracted considerable attention due to its favorable properties such as high coercive force, moderate saturation magnetization and high stability [29]. Recently it has been reported that metal nanoparticles supported on silica coated cobalt ferrite ($\text{M/SiO}_2\text{-CoFe}_2\text{O}_4$, $\text{M} = \text{Pd}$ [30], Ru [31], Ag [32], Cu [33]) provide high activity in hydrogen generation from the hydrolysis of ammonia borane. Herein, we report the synthesis and characterization of palladium(0) nanoparticles supported on polydopamine (PDA) coated cobalt ferrite powders, which were used as catalyst in hydrogen generation from the hydrolysis of ammonia borane. The synthesized $\text{Pd}^0/\text{PDA-}\text{CoFe}_2\text{O}_4$ is highly active catalyst providing a turnover frequency of $\text{TOF} = 175 \text{ min}^{-1}$ in hydrogen generation from the hydrolysis of ammonia borane at $25.0 \pm 0.1^\circ\text{C}$. On the other hand, palladium(0) nanoparticles supported on bare cobalt ferrite ($\text{Pd}^0/\text{CoFe}_2\text{O}_4$) are also highly active catalyst providing a TOF value of 290 min^{-1} . However, the reusability tests show that $\text{Pd}^0/\text{CoFe}_2\text{O}_4$ catalyst loses its activity in subsequent run, whereas $\text{Pd}^0/\text{PDA-}\text{CoFe}_2\text{O}_4$ catalyst retains its initial catalytic activity even after 10th use in the hydrolysis of ammonia borane releasing 3 equivalent H_2 per mole of AB.

2. Experimental

2.1. Materials

Cobalt ferrite particles (CoFe_2O_4 , 99%), palladium(II) nitrate hydrate ($\text{Pd}(\text{NO}_3)_2 \cdot x\text{H}_2\text{O}$), tris-HCl (Tris(hydroxymethyl) aminomethane hydrochloride, $\geq 99\%$), tris-base (Tris(hydroxymethyl) aminomethane, $\geq 99\%$), dopamine hydrochloride (99%), sodium borohydride (NaBH_4), ammonia borane (NH_3BH_3 or AB, 97%) were purchased from Sigma-Aldrich®. Distilled water was used for all the reactions obtained from Milli-Q water purification system.

2.2. Characterization

The crystallinity of the materials was studied by X-ray diffraction (XRD) by a MAC Science MXP 3TZ diffractometer using $\text{Cu K}\alpha$ radiation (wavelength 1.5406 \AA , 40 kV, 55 mA). The Fourier Transform Infrared (FTIR) spectra were recorded using Thermo Scientific, Nicolet iS5 FTIR coupled with Attenuated Total Reflectance (ATR). High resolution transmission electron microscopy (HRTEM), high angle annular dark-field scanning transmission electron microscopy (HAADF-STEM), and energy dispersive X-ray spectroscopy (EDX) were performed on FEI Tecnai G2 F30 or JEM-2100F (JEOL) transmission electron microscopes. Samples were examined at magnification between 400 K and 700 K. Surface composition and oxidation state of elements in all the catalysts were determined by Physical Electronics 5800 X-ray Photoelectron Spectroscopy (XPS) equipped with a hemispherical analyzer and using monochromatic $\text{Al K}\alpha$ radiation of 1486.6 eV, the X-ray tube working at 15 kV, 350 W and pass energy of 23.5 keV. Pd contents in the catalysts were determined by Inductively Coupled Plasma Optical Emission Spectroscopy (ICP-OES) (Leeman-Direct Reading Echelle) after dissolving each sample in the mixture of HNO_3/HCl (1:3 ratio). Surface area of the samples was determined by Brunauer-Emmett-Teller (BET) method using a Micromeritics ASAP2020 model. Nitrogen adsorption-desorption isotherm was recorded at -196°C . Before each adsorption, samples were out gassed at 150°C .

2.3. Synthesis of the catalysts

2.3.1. Polydopamine coated cobalt ferrite ($\text{PDA-}\text{CoFe}_2\text{O}_4$)

Polydopamine coated cobalt ferrite ($\text{PDA-}\text{CoFe}_2\text{O}_4$) was prepared by pH-induced self-polymerization process. Tris-buffer solution (10 mM, $\text{pH} = 8.5$) was prepared by adding appropriate amount of tris-HCl (44.2 mg) and tris-base (87.2 mg) in 100 mL H_2O . Cobalt ferrite powders (280 mg) were added into 50 mL tris-buffer solution containing 200 mg of dopamine hydrochloride (21 mM). The mixture was sonicated for 30 min and then stirred at room temperature for 72 h. The polydopamine coated nanoparticles were isolated by a permanent magnet, washed by distilled water and dried under vacuum at 60°C . The polymer thickness on the surface of CoFe_2O_4 was optimized by changing the dopamine hydrochloride salt concentration. 10.5, 21 and 42 mM of dopamine hydrochloride salt were used to prepare $\text{PDA-}\text{CoFe}_2\text{O}_4$ with different polymer thicknesses.

2.3.2. Palladium(0) nanoparticles supported on the surface of polydopamine coated cobalt ferrite ($\text{Pd}^0/\text{PDA-}\text{CoFe}_2\text{O}_4$)

Palladium(0) nanoparticles supported on polydopamine coated cobalt ferrite ($\text{Pd}^0/\text{PDA-}\text{CoFe}_2\text{O}_4$) were prepared by the impregnation of palladium(II) ions on the surface of $\text{PDA-}\text{CoFe}_2\text{O}_4$ followed by their reduction with sodium borohydride in aqueous solution at room temperature ($25.0 \pm 1.0^\circ\text{C}$). $\text{PDA-}\text{CoFe}_2\text{O}_4$ (100 mg) was dispersed in 50 mL of H_2O by ultrasonication for 5 min. Then appropriate amount of $\text{Pd}(\text{NO}_3)_2 \cdot x\text{H}_2\text{O}$ was added into this suspension and stirred at 500 rpm at room temperature ($25.0 \pm 1.0^\circ\text{C}$) for 24 h. Afterwards, aqueous NaBH_4 at a molar ratio of $\text{NaBH}_4/\text{Pd} = 5$ in 10 mL of H_2O was added drop wise into the mixed solution with vigorous stirring. After 1 h stirring, the sample ($\text{Pd}^0/\text{PDA-}\text{CoFe}_2\text{O}_4$) was isolated using a permanent magnet and washed with water and the remnant was dried under vacuum at 60°C for 12 h. For comparison, $\text{Pd}^0/\text{CoFe}_2\text{O}_4$ was also prepared by following the same procedure as described above, using CoFe_2O_4 instead of $\text{PDA-}\text{CoFe}_2\text{O}_4$.

2.4. Catalytic hydrolysis of ammonia borane

Hydrogen generation from the hydrolysis of ammonia borane was measured by water displacement method which was described elsewhere [34]. The reactor consists of a jacketed Schlenk tube (20 mL) which was connected to a water filled burette (60 cm in height and 3.0 cm in diameter) to measure the volume of the hydrogen gas to be evolved from the reaction (Fig. S1, see SI). The jacketed Schlenk tube was placed on a magnetic stirrer (Heidolph MR-301) and thermostated to $25.0 \pm 0.1^\circ\text{C}$ by circulating water to maintain the reaction temperature. The catalyst ($\text{Pd}^0/\text{PDA-}\text{CoFe}_2\text{O}_4$) was dispersed in 10 mL water in the Schlenk tube and 1.0 mmol $\text{H}_3\text{N-BH}_3$ (31.8 mg) was added into the reaction tube. The hydrolysis reaction was started by stirring the solution at 1200 rpm. The volume of the hydrogen gas evolved was measured in real time at constant atmospheric pressure. The catalytic activity of $\text{Pd}^0/\text{CoFe}_2\text{O}_4$ was also measured by the same procedure as described above.

2.5. Determination of the most active palladium loading of $\text{Pd}^0/\text{PDA-}\text{CoFe}_2\text{O}_4$ in the hydrolysis of ammonia borane

Palladium loading of the catalysts was optimized by synthesizing $\text{Pd}^0/\text{PDA-}\text{CoFe}_2\text{O}_4$ catalysts with different Pd loading. The catalytic activity of the synthesized $\text{Pd}^0/\text{PDA-}\text{CoFe}_2\text{O}_4$ samples with various palladium loadings in the range of 0.45–3.84 wt% was tested in hydrogen generation from the hydrolysis of ammonia borane starting with $\sim 0.94 \text{ mM Pd}$ and 100 mM AB in 10 mL

solution at 25.0 ± 0.1 °C. The highest catalytic activity was achieved by using 1.08 wt% palladium loaded PDA–CoFe₂O₄.

2.6. Catalytic hydrolysis of ammonia borane using Pd⁰/PDA–CoFe₂O₄ and Pd⁰/CoFe₂O₄ at different Pd concentrations

The kinetic study of the hydrolysis reaction was carried out using Pd⁰/PDA–CoFe₂O₄ and Pd⁰/CoFe₂O₄ catalysts at different palladium concentrations in the range 0.06–1.00 mM Pd with 100 mM AB in 10 mL of water at 25.0 ± 0.1 °C.

2.7. Determination of activation energy for the hydrolysis of ammonia borane catalyzed by Pd⁰/PDA–CoFe₂O₄ and Pd⁰/CoFe₂O₄

To determine the activation energy of hydrolysis of ammonia borane in presence of the synthesized catalysts, the hydrolysis reaction was performed starting with 10 mL of 100 mM (31.8 mg) AB solution and 25 mg of Pd⁰/PDA–CoFe₂O₄ (1.08 wt% Pd) at various temperatures (25, 30, 35 and 40 °C). The rate for the hydrogen generation reaction was calculated from the slope of the linear part of each hydrogen evolution versus time plot at various temperatures. Activation energy for the hydrolysis of ammonia borane catalyzed by Pd⁰/PDA–CoFe₂O₄ was obtained from the slope of Arrhenius plot. For comparison, the same experiment was performed using 10 mg of Pd⁰/CoFe₂O₄ (1.17 wt% Pd) catalyst. Since the catalytic activity of the uncoated catalyst is very high as compared to the coated one, lower amount of the catalyst was used.

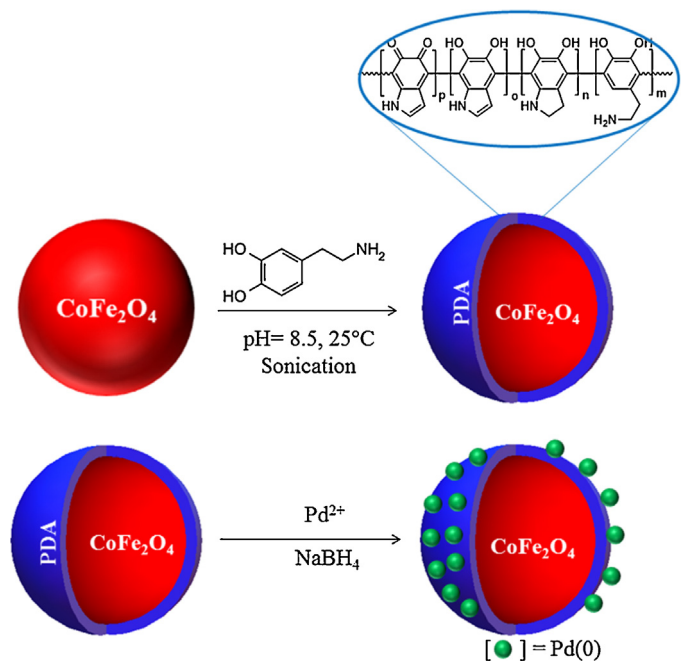
2.8. Reusability of Pd⁰/PDA–CoFe₂O₄ and Pd⁰/CoFe₂O₄ in the hydrolysis of ammonia borane

A set of experiments were performed to observe whether the synthesized catalysts are reusable or not in AB hydrolysis reaction. After the complete hydrolysis of AB started with 10 mL of 100 mM AB (31.8 mg H₃N.BH₃), and 50 mg Pd⁰/PDA–CoFe₂O₄ (1.08 wt% Pd, [Pd] = 0.5 mM) at 25.0 ± 0.1 °C, the catalyst was isolated by a permanent magnet, washed with water and redispersed in 10 mL solution of 100 mM AB for a subsequent run of hydrolysis at 25.0 ± 0.1 °C. For comparison, reusability tests were also performed for Pd⁰/CoFe₂O₄ catalyst by the same procedure using 50 mg catalyst (1.17 wt% Pd, [Pd] = 0.55 mM) at 25.0 ± 0.1 °C.

3. Results and discussion

CoFe₂O₄ particles were coated with polydopamine by pH-induced polymerization of dopamine hydrochloride in Tris-buffer solution at room temperature [35]. The dopamine salt concentration was optimized to obtain an efficient coating. The dopamine salt concentration of 21 mM was found to provide the most effective coating for the cobalt ferrite particles. Polydopamine coated cobalt ferrite (PDA–CoFe₂O₄) has the capability to coordinate metal ions or atoms through the N- and O-binding sites on the surface of polymeric layer [36]. Thus, palladium(0) nanoparticles supported on polydopamine coated cobalt ferrite (Pd⁰/PDA–CoFe₂O₄) could be prepared by impregnation of palladium(II) ions on the surface of polymer layer followed by their reduction with sodium borohydride (Scheme 1). Pd⁰/PDA–CoFe₂O₄ was magnetically isolated from the reaction solution and characterized by using a combination of advanced analytical techniques including XRD, HAADF-STEM, EDS, BET, XPS, FTIR, and ICP-OES.

The XRD patterns of CoFe₂O₄, PDA–CoFe₂O₄ and Pd⁰/PDA–CoFe₂O₄ (Pd loading 1.08 wt%) in Fig. 1 exhibit peaks at 30.38°, 35.77°, 43.37°, 53.91°, 57.20°, and 62.95° which can be attributed to (220), (311), (400), (422), (511), and (440) diffractions of CoFe₂O₄, respectively (JCPDS card no. 22-1086). The



Scheme 1. Synthesis of palladium(0) nanoparticles supported on polydopamine coated cobalt ferrite (Pd⁰/PDA–CoFe₂O₄).

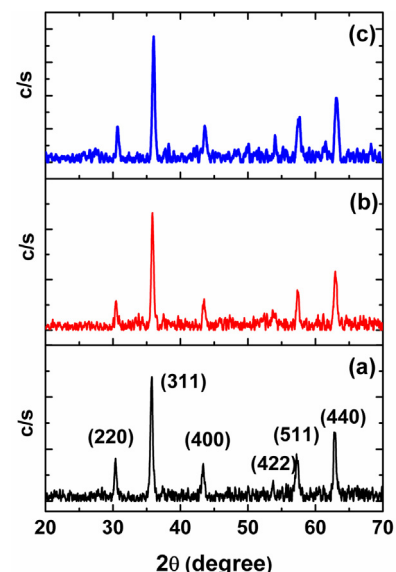


Fig. 1. Powder XRD patterns of (a) CoFe₂O₄, (b) PDA–CoFe₂O₄, and (c) Pd⁰/PDA–CoFe₂O₄ with a 1.08 wt% Pd loading.

diffraction pattern of cobalt ferrite shows a cubic spinel lattice for CoFe₂O₄ ($Fd\bar{3}m$ -277: $a = b = c = 8.234$ Å) [37]. Comparison of the diffraction patterns of the Pd⁰/CoFe₂O₄ and Pd⁰/PDA–CoFe₂O₄ samples indicate that there is no phase change in the CoFe₂O₄ lattice after PDA coating or Pd loading. Although the presence of palladium(0) nanoparticles on the surface of PDA–CoFe₂O₄ were confirmed by other techniques (EDX, XPS) there is no observable peak attributable to palladium in Fig. 1c, most likely because of the low palladium loading on the support.

The HAADF-STEM and corresponding palladium particle size histogram for Pd⁰/PDA–CoFe₂O₄ catalyst with a palladium loading of 1.08 wt% (Fig. 2) show that (i) the cobalt ferrite particles are evenly coated by polydopamine, (ii) palladium(0) nanoparticles are well dispersed on the surface of the PDA–CoFe₂O₄, and

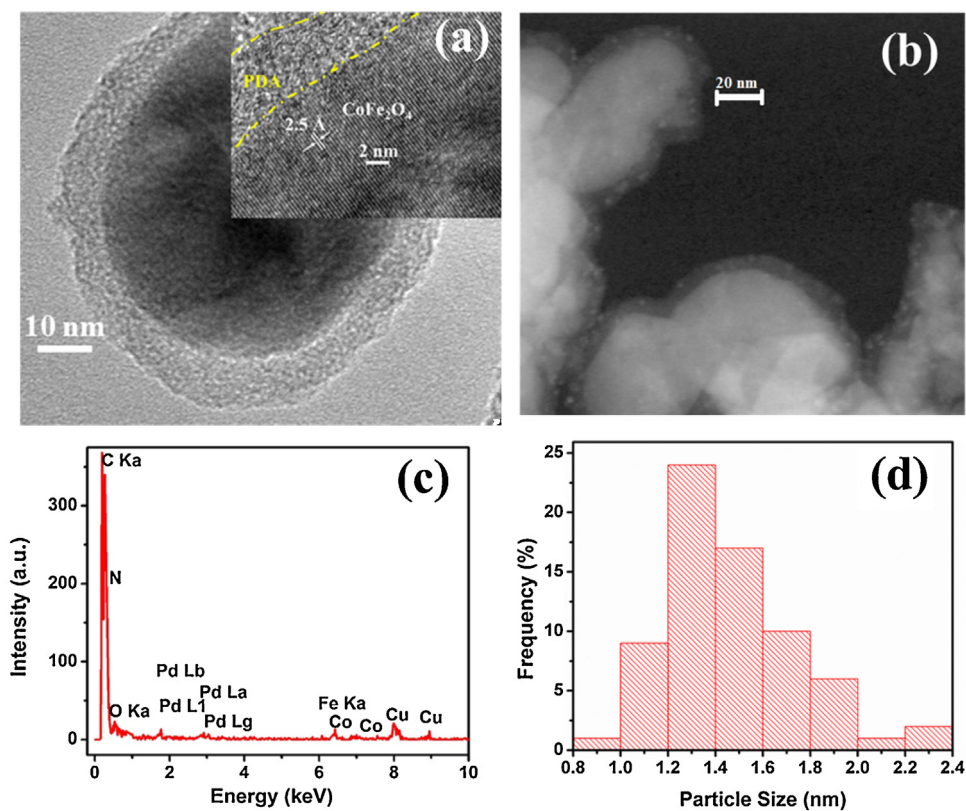


Fig. 2. HAADF-STEM images of $\text{Pd}^0/\text{PDA}-\text{CoFe}_2\text{O}_4$ (1.08 wt% Pd) showing (a) dopamine layer and lattice fringes (inset), (b) Palladium NPs on the dopamine layer, (c) TEM-EDS spectrum of $\text{Pd}^0/\text{PDA}-\text{CoFe}_2\text{O}_4$ (1.08 wt% Pd) and (d) the histogram showing the particle size distribution of palladium(0) nanoparticles.

(iii) the size of palladium(0) nanoparticles formed on the surface of the $\text{PDA}-\text{CoFe}_2\text{O}_4$ is in the range 0.8–2.4 nm (mean diameter: 1.4 ± 0.3 nm). EDS spectrum in Fig. 2c shows the presence of Pd, C, N, Co, Fe and O elements, which confirms the successful PDA coating of CoFe_2O_4 as well as successful loading of Pd on the surface of $\text{PDA}-\text{CoFe}_2\text{O}_4$. Average thickness of the PDA layer was observed to be 8.6 ± 1.0 nm on the surface of cobalt ferrite particles (Fig. 2a). The lattice fringe of $\text{PDA}-\text{CoFe}_2\text{O}_4$ (the inset in Fig. 2a) reveals the d -spacing (0.25 nm) of (311) spinel planes of the cobalt ferrite crystal phase [38].

Surface area of the cobalt ferrite powders is $55.73 \text{ m}^2 \text{ g}^{-1}$ as measured by BET analysis. The surface area of CoFe_2O_4 particles expectedly decreases to $47.39 \text{ m}^2 \text{ g}^{-1}$ after PDA coating and to $42.83 \text{ m}^2 \text{ g}^{-1}$ upon palladium loading.

The surface composition and oxidation states of the elements of the $\text{Pd}^0/\text{PDA}-\text{CoFe}_2\text{O}_4$ catalyst were analyzed by XPS (Fig. 3). The survey-scan XPS spectrum of $\text{Pd}^0/\text{PDA}-\text{CoFe}_2\text{O}_4$ catalyst (Fig. 3a) shows the presence of Pd in addition to the framework elements (Co, Fe, C, N, O) in line with the EDS result. The XPS scans for $\text{Pd}3\text{d}$, $\text{C}1\text{s}$ and $\text{N}1\text{s}$ core of $\text{Pd}^0/\text{PDA}-\text{CoFe}_2\text{O}_4$ sample are also given in Fig. 3b–d, respectively. The $\text{Pd}3\text{d}$ spectrum (Fig. 3b) shows two prominent peaks at 339.8 and 334.68 eV which can readily be assigned to $\text{Pd}(0) 3\text{d}_{3/2}$ and $3\text{d}_{5/2}$, respectively, by comparing with the values of metallic palladium [39]. The bands at 341.7 and 336.3 eV can be attributed to the $\text{Pd}(\text{II}) 3\text{d}_{3/2}$ and $3\text{d}_{5/2}$, respectively [40], which may be formed from the partial oxidation of palladium(0) nanoparticles upon air exposure during XPS sampling. Three peaks in the $\text{C}1\text{s}$ spectrum (Fig. 3c) at 284.3, 285.5 eV, and 287.5 eV can be assigned to the $\text{CH}_x/\text{C}-\text{NH}_2$, $\text{C}-\text{N/C}-\text{O}$ and $\text{C}=\text{O}$ groups of polydopamine, respectively [41]. The peaks at 398.0, 399.6, and 401.7 eV in the $\text{N}1\text{s}$ spectrum (Fig. 3d) are attributable to $=\text{NR}$, R_2NH and RNH_2 groups of the polydopamine, respectively [42]. Thus, XPS spectra of $\text{C}1\text{s}$ and $\text{N}1\text{s}$ provide further evidence

for the successful coating of CoFe_2O_4 particles with polydopamine, which was also confirmed by FTIR analysis (Fig. S2 in the SI).

Before the detailed investigation on the kinetics of the catalytic reaction, the effect of dopamine layer thickness on the surface of CoFe_2O_4 was studied. PDA was coated on CoFe_2O_4 by using dopamine hydrochloride at different concentrations (10.5, 21 and 42 mM), which resulted in the formation of PDA layer with different thicknesses on the surface of CoFe_2O_4 . After the synthesis of $\text{Pd}^0/\text{PDA}-\text{CoFe}_2\text{O}_4$ support from different dopamine salt concentration, $\text{Pd}^0/\text{PDA}-\text{CoFe}_2\text{O}_4$ catalysts with a palladium loading of 3.84 wt% were prepared and used in hydrogen generation from the hydrolysis of AB at $25.0 \pm 0.1^\circ\text{C}$ starting with 10 mL aqueous solution of 1.0 mmol AB and 25 mg $\text{Pd}^0/\text{PDA}-\text{CoFe}_2\text{O}_4$ catalyst ($[\text{Pd}] = 0.94 \text{ mM}$). From the HAADF-STEM images in Fig. 4c–e, the thickness of PDA layer formed on the surface of cobalt ferrite nanopowders can be estimated to be 6.0 ± 0.7 , 8.6 ± 1.0 and 10.2 ± 0.9 nm for $\text{Pd}^0/\text{PDA}-\text{CoFe}_2\text{O}_4$ prepared using 10.5, 21, 42 mM dopamine salt concentration, respectively. The STEM images in Fig. 4c–e also shows that palladium(0) nanoparticles are well dispersed on the surface of $\text{PDA}-\text{CoFe}_2\text{O}_4$ in all three samples. The catalytic activity of $\text{Pd}^0/\text{PDA}-\text{CoFe}_2\text{O}_4$ catalysts shows variation with the polymer thickness. The highest catalytic activity is provided by $\text{Pd}^0/\text{PDA}-\text{CoFe}_2\text{O}_4$ catalyst with a PDA thickness of 8.6 ± 1.0 nm (Fig. 4a and b). The catalytic activity of the catalysts with different dopamine thicknesses shows variation due to the formation of different size of palladium nanoparticles in each of the samples. The mean size of palladium(0) nanoparticles formed on the surface of PDA layers are found to be 3.5 ± 0.7 , 2.8 ± 0.5 and 3.0 ± 0.6 nm on the surface of PDA coat with thickness of 6.0, 8.6 and 10.2 nm, respectively (Fig. 5). For lower PDA thickness, the size of the Pd nanoparticles is observed to be larger, which results in lower catalytic activity. On the other hand, with the increase in the PDA thickness, the interaction palladium with

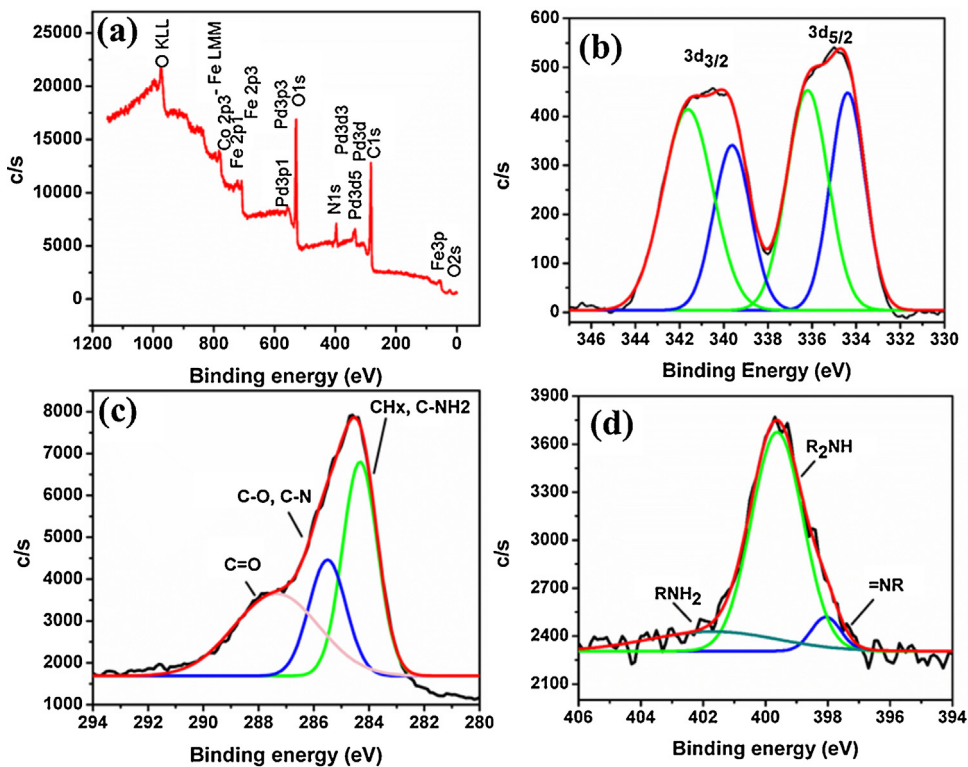


Fig. 3. (a) X-ray photoelectron survey spectrum of $\text{Pd}^0/\text{PDA}-\text{CoFe}_2\text{O}_4$ (1.08 wt% Pd) and high resolution scan XPS of (b) Pd3d, (c) C1s, and (d) N1s core-levels.

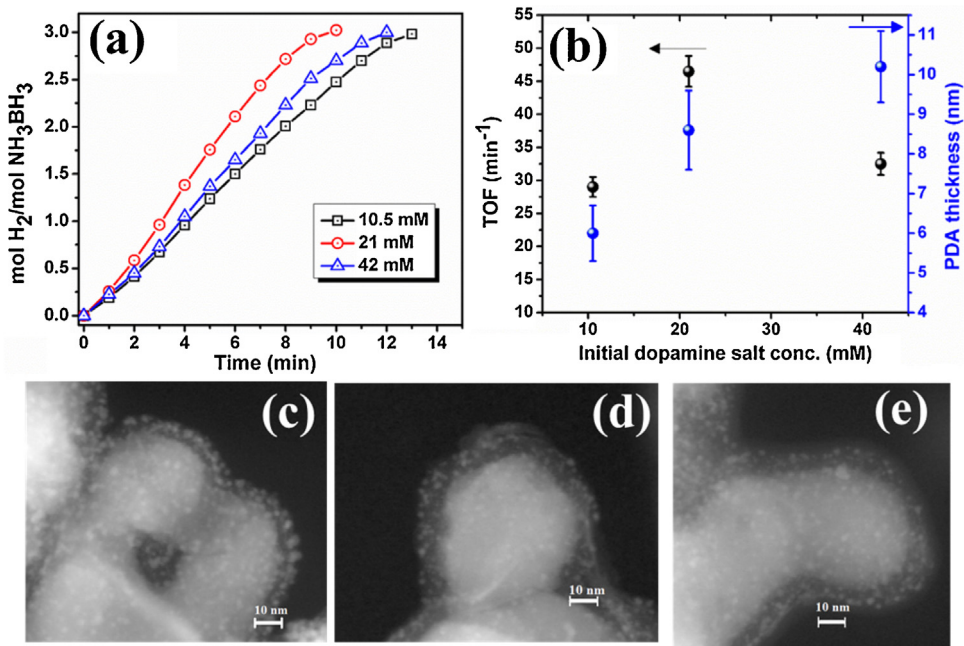


Fig. 4. (a) Equivalent H_2 versus time plot for hydrogen generation from the hydrolysis of ammonia borane (0.10 M) in presence of $\text{Pd}^0/\text{PDA}-\text{CoFe}_2\text{O}_4$ (3.81 wt% Pd) catalysts synthesized from various initial dopamine salt concentration at $25.0 \pm 0.1^\circ\text{C}$, (b) TOF values versus polymer thickness at different dopamine salt concentrations and the TEM images of $\text{Pd}^0/\text{PDA}-\text{CoFe}_2\text{O}_4$ (3.81 wt% Pd) catalyst synthesized using (c) 10.5 mM, (d) 21 mM and (e) 42 mM dopamine salt concentration.

the CoFe_2O_4 core becomes less, and accordingly the catalyst with 10.2 nm PDA thickness showed lower activity. It is also noteworthy that the $\text{PDA}-\text{CoFe}_2\text{O}_4$ particles with a 10.2 nm polymer coat, remain suspended in the solution for more than an hour despite the use of a strong magnet. This is likely due to thick polymer layer having reduced magnetic susceptibility. Consequently, we

decided to use 8.6 nm PDA coated support for the preparation of $\text{Pd}^0/\text{PDA}-\text{CoFe}_2\text{O}_4$ catalysts for the further studies.

Next, a series of experiments were performed at $25.0 \pm 0.1^\circ\text{C}$ starting with 10 mL aqueous solution of 1.0 mmol AB and $\text{Pd}^0/\text{PDA}-\text{CoFe}_2\text{O}_4$ catalysts with various Pd loading (0.45, 1.08, 1.96, 3.07, and 3.84 wt% Pd) in appropriate amount to provide

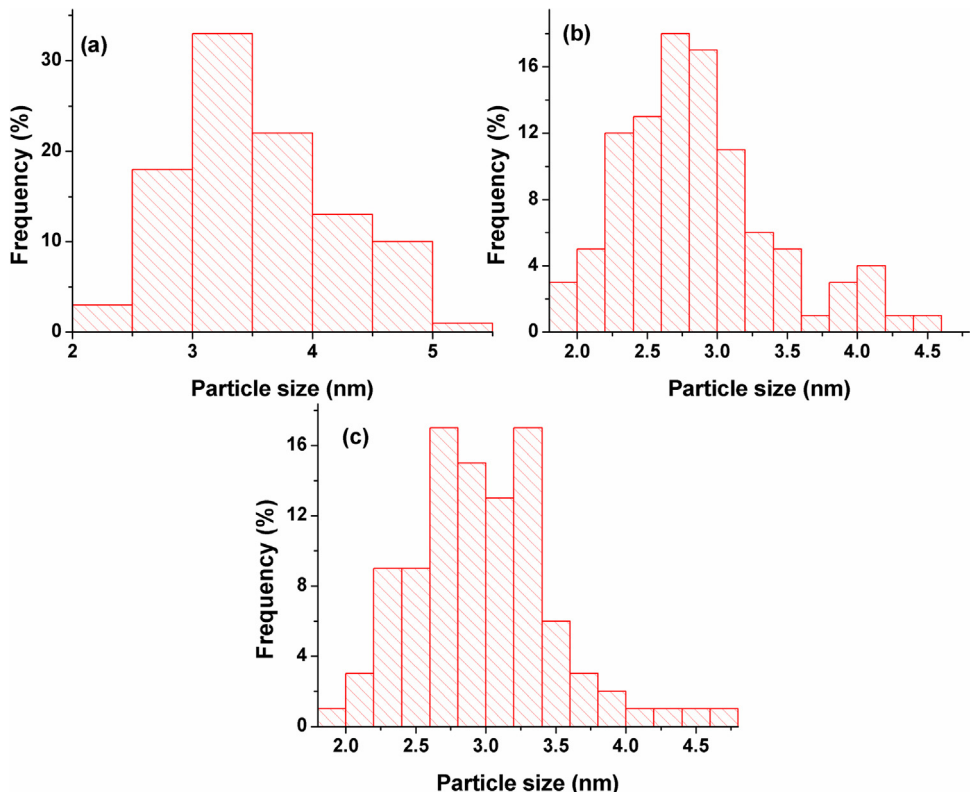


Fig. 5. Particle size distribution histogram of Pd(0) nanoparticles on the surface of PDA coated CoFe₂O₄ (3.84 wt% Pd) prepared using (a) 10.5 mM, (b) 21 mM, and (c) 42 mM dopamine salt and the mean size of palladium(0) nanoparticles is 3.5 ± 0.7 , 2.8 ± 0.5 , and 3.0 ± 0.6 nm, respectively.

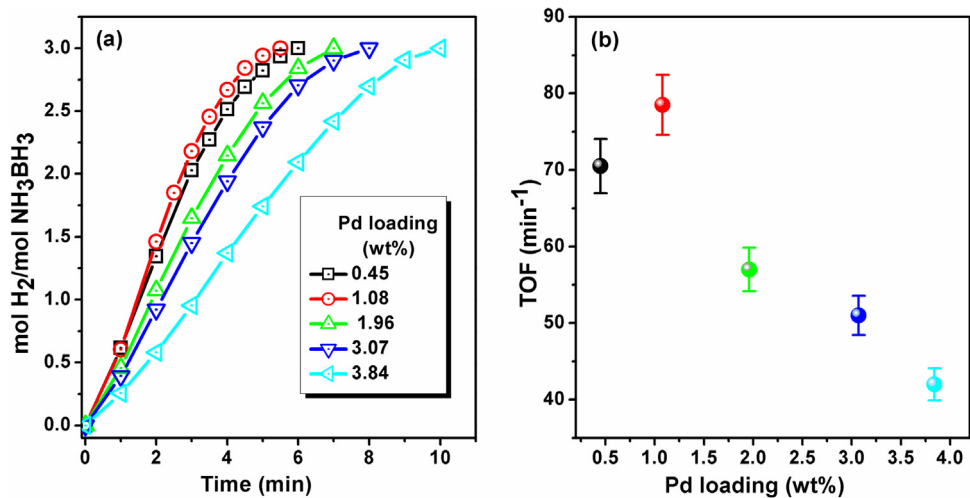


Fig. 6. (a) Equivalent H₂ versus time plot for hydrogen generation from the hydrolysis of ammonia borane performed with 0.10 M AB, 0.94 mM Pd in 10.0 mL water at 25.0 ± 0.1 °C in presence of Pd⁰/PDA–CoFe₂O₄ catalysts with various palladium loadings and (b) the corresponding TOF values.

the same Pd concentration ($[Pd] = \sim 0.94$ mM) in all of the experiments. The Pd⁰/PDA–CoFe₂O₄ sample with palladium loading of 1.08 wt% Pd provides the highest catalytic activity in hydrogen generation from the hydrolysis of AB at 25.0 ± 0.1 °C (Fig. 6). As the palladium loading further increases, the catalytic activity of Pd⁰/PDA–CoFe₂O₄ decreases, most probably due to the formation of larger palladium(0) nanoparticles as seen from the comparison of the histograms in Figs. 2d and 5 [43]. For all the tests and characterization reported hereafter, Pd⁰/PDA–CoFe₂O₄ catalysts with palladium loading of 1.08 wt% was used.

Before proceeding with the investigation on the catalytic activity of Pd⁰/PDA–CoFe₂O₄, a set of control experiments were

performed to check the catalytic activity of supporting materials in the hydrolysis of ammonia borane. Fig. 7 gives the plot of hydrogen release versus time for the hydrolysis of ammonia borane in the presence of CoFe₂O₄, Pd⁰/CoFe₂O₄, PDA–CoFe₂O₄, or Pd⁰/PDA–CoFe₂O₄ at 25.0 ± 0.1 °C. The hydrogen generation plots in Fig. 7 show that CoFe₂O₄ and PDA–CoFe₂O₄ are catalytically silent in the hydrolysis of AB for 18 h, while Pd⁰/CoFe₂O₄ and Pd⁰/PDA–CoFe₂O₄ are highly active catalysts providing TOF values of 290 and 175 min⁻¹, respectively, in releasing 3 equivalent H₂ per mole of AB at 25.0 ± 0.1 °C. It is noteworthy that Pd⁰/CoFe₂O₄ has higher catalytic activity than that of the Pd⁰/PDA–CoFe₂O₄ catalyst. The higher catalytic activity of Pd⁰/CoFe₂O₄ may be attributed to

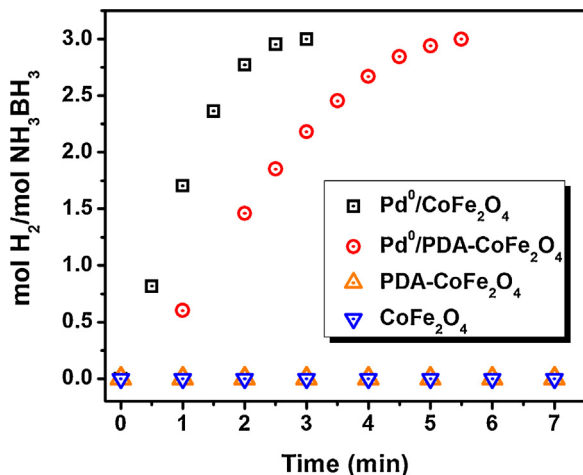


Fig. 7. Equivalent H_2 versus time plot for hydrogen generation from the hydrolysis of ammonia borane (0.10 M) in presence of $CoFe_2O_4$, $PDA-CoFe_2O_4$, $Pd^0/CoFe_2O_4$ (1.17 wt% Pd) and $Pd^0/PDA-CoFe_2O_4$ (1.08 wt% Pd) at $25.0 \pm 0.1^\circ C$.

the strong metal–support interaction in the $Pd-Co^{II}Fe^{III}_2O_4$ system. The mechanism of the promoting effect of oxides has not been well defined yet. In a recent publication, Bruix et al. have explained the metal–support interaction in terms of electronic perturbation for $Pt-CeO_2$ catalyst [44]. Similar metal–support interaction has also been reported for electron rich late transitional metal nanoparticles supported on other oxides (CeO_2 [45], TiO_2 [46], Co_3O_4 [47], MnO_2 [48], ZnO [49], etc.). A comparison of the catalytic activities of $Pd^0/CoFe_2O_4$ and $Pd^0/PDA-CoFe_2O_4$ catalysts with the literature TOF value of 254 min^{-1} for $Pd^0/SiO_2-CoFe_2O_4$ [30] would not be fair as different cobalt ferrite cores have been used in preparing

the palladium catalysts: While magnetic $CoFe_2O_4$ has been prepared by wet chemical method using iron(III) and cobalt(II) chloride in the previous study [30], we used the commercial cobalt ferrite with an average particle size of 30 nm in the preparation of catalysts. In order to make the results comparable, $Pd^0/SiO_2-CoFe_2O_4$ was also prepared starting with the same commercial cobalt ferrite as the one used in this study (see SI). The TOF value for the new $Pd^0/SiO_2-CoFe_2O_4$ catalyst with the same commercial cobalt ferrite is now 20 min^{-1} (Fig. 8c) which is much smaller than that reported previously which has been reported to have large surface area of $178\text{ m}^2\text{ g}^{-1}$ [30]. The lower catalytic activity of $Pd^0/SiO_2-CoFe_2O_4$ compared to that of $Pd^0/PDA-CoFe_2O_4$ catalyst is likely due to the larger particle size and partial aggregation of palladium(0) nanoparticles on the silica layer (Fig. 8a and b).

The mechanism of hydrogen generation from the catalytic hydrolysis of ammonia borane in the presence of transition metal nanoparticles has been well established [50]. NH_3BH_3 molecule interacts with active sites on the surface of transition metal nanoparticles through the hydridic hydrogen atoms of BH_3 group forming an activated complex, whereby the B–N bond is weakened and undergoes dissociation upon the attack of water molecule. The resulting BH_3 intermediate undergoes hydrolysis stepwise to form the ultimate borate ion and releases a total of 3 equivalents of H_2 per mole ammonia borane [51].

Further kinetic studies were performed using both $Pd^0/CoFe_2O_4$ (1.17 wt% Pd) and $Pd^0/PDA-CoFe_2O_4$ (1.08 wt% Pd) catalysts at $25.0 \pm 0.1^\circ C$. Fig. 9a and b shows the plots of equivalent H_2 per mole of AB versus time during the catalytic hydrolysis of AB for $Pd^0/CoFe_2O_4$ and $Pd^0/PDA-CoFe_2O_4$ catalysts, respectively, in different Pd concentrations at $25.0 \pm 0.1^\circ C$. The hydrogen generation starts immediately without noticeable induction period and continues almost linearly until the consumption of all ammonia borane

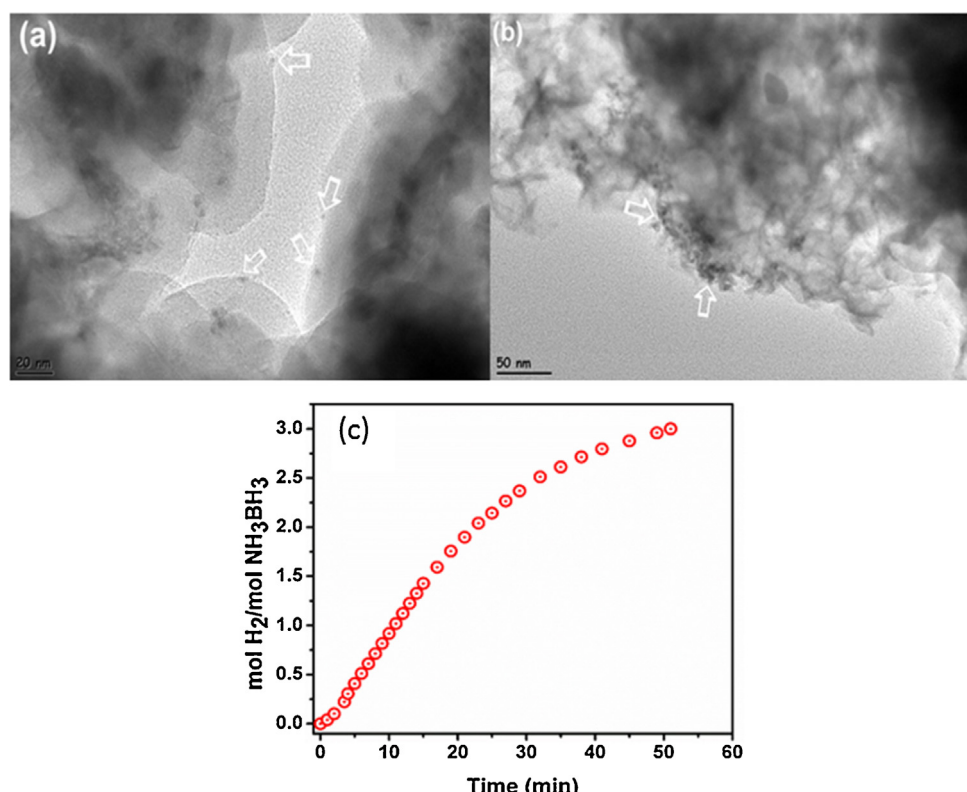


Fig. 8. (a and b) TEM images of $Pd^0/SiO_2-CoFe_2O_4$ (1.0 wt% Pd) at different magnifications (Pd particle size is in the range between 3.0 and 6.0 nm), and (c) equivalent H_2 versus time plot for hydrogen generation from the hydrolysis of ammonia borane performed with 0.10 M AB, 0.47 mM Pd in 10.0 mL water at $25.0 \pm 0.1^\circ C$ in presence of $Pd^0/SiO_2-CoFe_2O_4$ (1.0 wt% Pd).

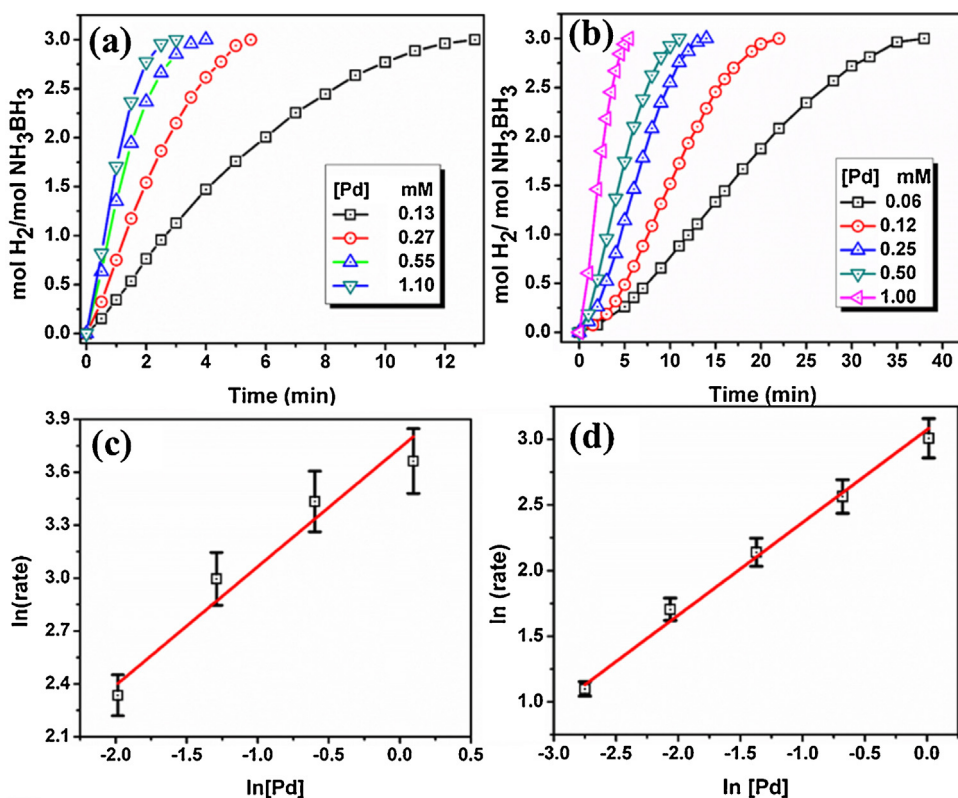


Fig. 9. Plots of equivalent H_2 per mole of AB versus time during the catalytic hydrolysis of ammonia borane (0.10 M) using (a) $\text{Pd}^0/\text{CoFe}_2\text{O}_4$ catalyst (1.17 wt% Pd) and (c) $\text{Pd}^0/\text{PDA}-\text{CoFe}_2\text{O}_4$ catalyst (1.08 wt% Pd) at different palladium concentrations at $25.0 \pm 0.1^\circ\text{C}$. The logarithmic plot of hydrogen generation rate versus the palladium concentration for (b) $\text{Pd}^0/\text{CoFe}_2\text{O}_4$ catalyst, $\ln(\text{rate}) = 0.68 \ln[\text{Pd}] + 3.74$ and (d) $\text{Pd}^0/\text{PDA}-\text{CoFe}_2\text{O}_4$ catalyst, $\ln(\text{rate}) = 0.70 \ln[\text{Pd}] + 3.07$.

Table 1

Catalytic activity of reported palladium catalysts in hydrogen generation from the hydrolysis of ammonia borane at $25.0 \pm 1.0^\circ\text{C}$.

Catalyst	Surface area ($\text{m}^2 \text{g}^{-1}$)	Average Pd particle size (nm)	TOF (min^{-1})	Metal/AB (mol/mol)	E_a (kJ mol $^{-1}$)	Retained activity after reusing	Ref.
$\text{Pd}^0/\text{CoFe}_2\text{O}_4^{\text{a}}$	55.7	2.7	290	0.0014	42	90% at 5th run	This study
$\text{Pd}^0/\text{SiO}_2-\text{CoFe}_2\text{O}_4^{\text{a}}$	171.3	6.0	254	0.0186	52	100% at 10th run	[30]
$\text{Pd}^0/\text{PDA}-\text{CoFe}_2\text{O}_4^{\text{a}}$	42.8	1.4	175	0.0006	65	100% at 10th run	This study
4 wt% Pd@MIL-101	1603.0	1.8	45	0.0189	–	100% at 5th run ^b	[52]
Pd@Co/graphene ^a	–	7.0	37.5	0.09	–	97% after 5th run ^b	[53]
$\text{Co}_{35}\text{Pd}_{65}/\text{C}$ annealed ^a	–	–	35.7	0.024	–	–	[54]
$\text{RGO}-\text{Cu}_{75}\text{Pd}_{25}$	–	3.0	29.9	0.003	45	90% at 3rd run	[55]
Pd/CeO ₂	–	4.0	29	0.011	68	47% at 5th run	[6]
RGO@Pd	500.0	–	26.3	0.06	40	95% at 10th run	[60]
$\text{Co}_{35}\text{Pd}_{65}/\text{C}^{\text{a}}$	–	8.0	22.7	0.024	27.5	100% at 3rd run ^b	[54]
CDG-Pd	500.0	4.5	15.5	0.005	–	95% at 10th run	[56]
$\text{Pd}^0/\text{PDA}-\text{Fe}_3\text{O}_4^{\text{a}}$	41.78	2.0	14.5	0.009	65	100% at 10th run	[34]
$\text{Pd}_{69}\text{Sn}_{31}$ NPs/C	–	6.5	13.64	0.0275	27.2	~90% at 6th run ^{b,c}	[57]
Pd/SiO ₂	–	–	10	0.0186	–	–	[30]
Pd-HAP	–	3.3	8.3	0.02	55	88% at 5th run	[58]
Pd/nanoTiO ₂	–	–	7.1	0.0228	–	–	[6]
Pd/nanoSiO ₂	–	–	6.6	0.0228	–	–	[6]
Pd/zeolite	682.0	–	6.25	0.02	56	92% at 5th run	[62]
RGO/Pd	–	4.0	6.25	0.04	51	65% at 5th run ^b	[59]
Pd-PVB-TiO ₂	–	–	6	0.06	55.9	89% at 5th run	[61]
$\text{Pd}^0/\text{Fe}_3\text{O}_4^{\text{a}}$	–	–	5.5	0.009	–	–	[34]
$\text{Pd}^0/\text{SiO}_2-\text{Fe}_3\text{O}_4^{\text{a}}$	–	–	5	0.009	–	–	[34]
PSSA-co-MA-Pd	–	3.5	5	0.02	44	–	[63]
Pd/nanoAl ₂ O ₃	–	–	3.5	0.0228	–	–	[6]
Pd/nanoZrO ₂	–	–	3.5	0.0228	–	–	[6]
2% Pd/ γ -Al ₂ O ₃	37.0	3.6	1.39	0.025	–	–	[22]
Pd black	–	–	0.67	0.05	–	–	[64]

^a Magnetically isolable catalysts.

^b AB added into the reactor without removing the solution in recyclability tests.

^c Activity calculated from the given data.

present in the solution. Plotting the hydrogen generation rate versus the initial concentration of palladium, both in logarithmic

scales (Fig. 9c and d) gives straight line with a slope of ~0.7 for both of the catalysts in the hydrolysis of ammonia borane. Highest

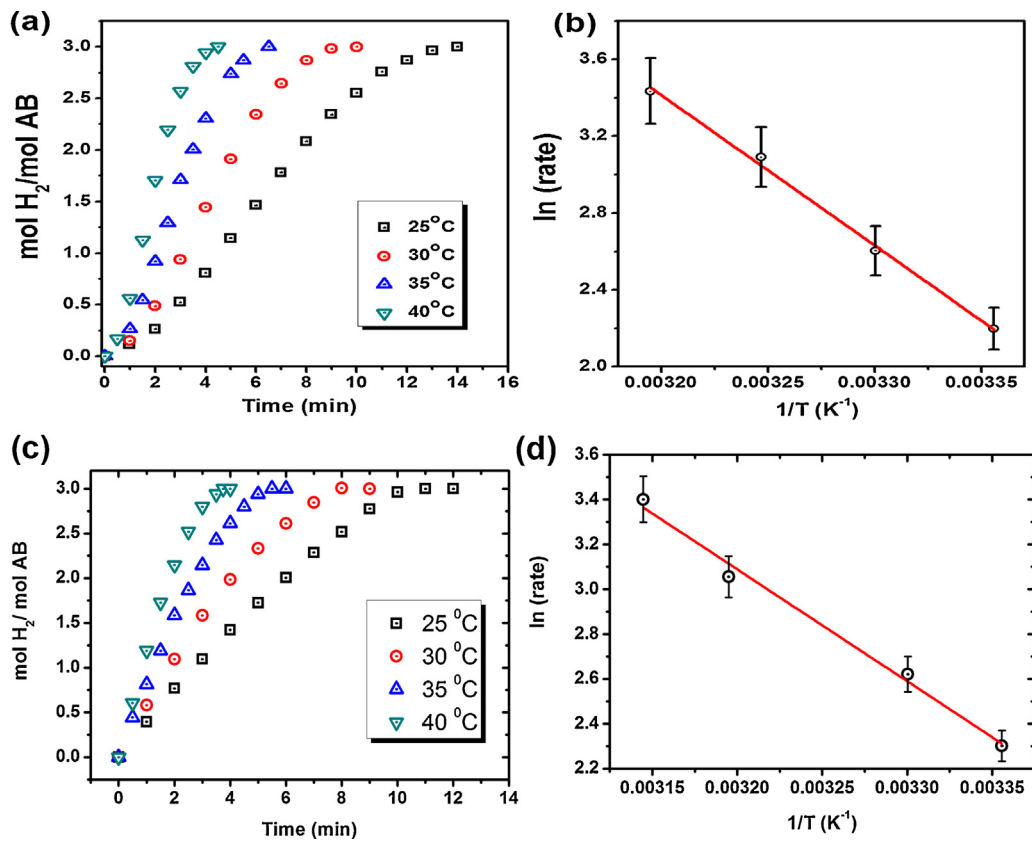


Fig. 10. Plots of equivalent H₂ per mole of AB versus time during the catalytic hydrolysis of ammonia borane (0.10 M) using the Pd⁰/PDA-CoFe₂O₄ catalyst (1.08 wt% Pd) (a) and Pd⁰/CoFe₂O₄ catalyst (1.17 wt% Pd) (c) for hydrogen generation from the hydrolysis of AB at various temperatures. Arrhenius plots for the catalytic hydrolysis of ammonia borane for Pd⁰/PDA-CoFe₂O₄ catalyst, ln(rate) = 28.48–7835/T (b) and Pd⁰/CoFe₂O₄ catalyst, ln(rate) = 19.05–4988/T (d).

TOF values for Pd⁰/CoFe₂O₄ and Pd⁰/PDA-CoFe₂O₄ catalysts are found to be 290 and 175 min⁻¹, respectively. The TOF values of Pd⁰/CoFe₂O₄ and Pd⁰/PDA-CoFe₂O₄ catalysts are compared with the reported TOF values of other Pd based catalysts given in Table 1 such as Pd/SiO₂–CoFe₂O₄ [30], Pd@MIL-101 [52], Pd@Co/graphene [53], Co₃₅Pd₆₅/C [54], RGO–Cu₇₅Pd₂₅ [55], CDG–Pd [56], Pd₆₉Sn₃₁ NPs/C [57], Pd–HAP [58], RGO/Pd [59], 2.1 wt% RGO@Pd [60], Pd–PVB–TiO₂ [61], Pd/zeolite [62], PSSA–co–MA–Pd [63] and Pd black [64]. The comparison of the catalytic activity of catalyst reported in literature for the hydrolysis of AB in terms of TOF listed in Table 1

shows that there is no clear insight in explaining the catalytic activity depending on the type of supporting material, surface area of the catalyst and the particle size of palladium nanoparticles.

Activation energy (E_a) of the hydrolysis of ammonia borane catalyzed by Pd⁰/PDA-CoFe₂O₄ with a palladium loading of 1.08 wt% Pd can be calculated from the Arrhenius plot constructed using hydrogen generation rates at various temperatures in the range between 25.0–40.0 °C (Fig. 10). The apparent rate constants of AB hydrolysis reactions at different temperatures were calculated from the slope of initial linear region of each plot and used

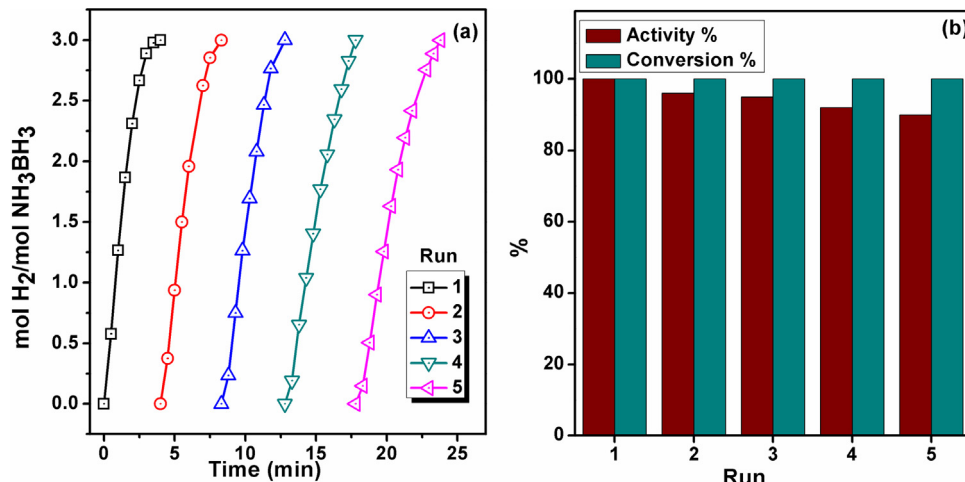


Fig. 11. (a) Plots of equivalent H₂ per mole of AB versus time in successive runs of catalytic hydrolysis of ammonia borane (0.10 M) starting with 50 mg of Pd⁰/CoFe₂O₄ catalyst (1.17 wt% Pd) at 25.0 ± 0.1 °C and (b) the corresponding percent initial catalytic activity and the percent conversion of AB for each run.

to construct Arrhenius plot in Fig. 10b. The apparent activation energy was calculated to be $E_a = 65 \pm 3 \text{ kJ mol}^{-1}$. The obtained activation energy for the hydrolysis of ammonia borane catalyzed by $\text{Pd}^0/\text{PDA-Fe}_2\text{O}_4$ is comparable to the literature values reported for the other palladium-based catalysts (Table 1). For comparison, the activation energy of the hydrolysis of ammonia borane catalyzed by $\text{Pd}^0/\text{CoFe}_2\text{O}_4$ (1.17 wt% Pd) was also determined to be $E_a = 42 \pm 2 \text{ kJ mol}^{-1}$ (Fig. 10c and d). Although one is tempted to

see a relation between the activation energy and TOF values of the catalysts, further investigation is needed for a concrete suggestion.

Reusability, an important criterion in judging the catalytic performance, is usually measured as the relative activity maintained in successive runs of catalytic reaction performed using the catalyst isolated after the previous run. Thereby, the catalyst isolation is usually achieved by filtration/centrifugation. The tedious process of catalysts separation by filtration or centrifugation is not only time

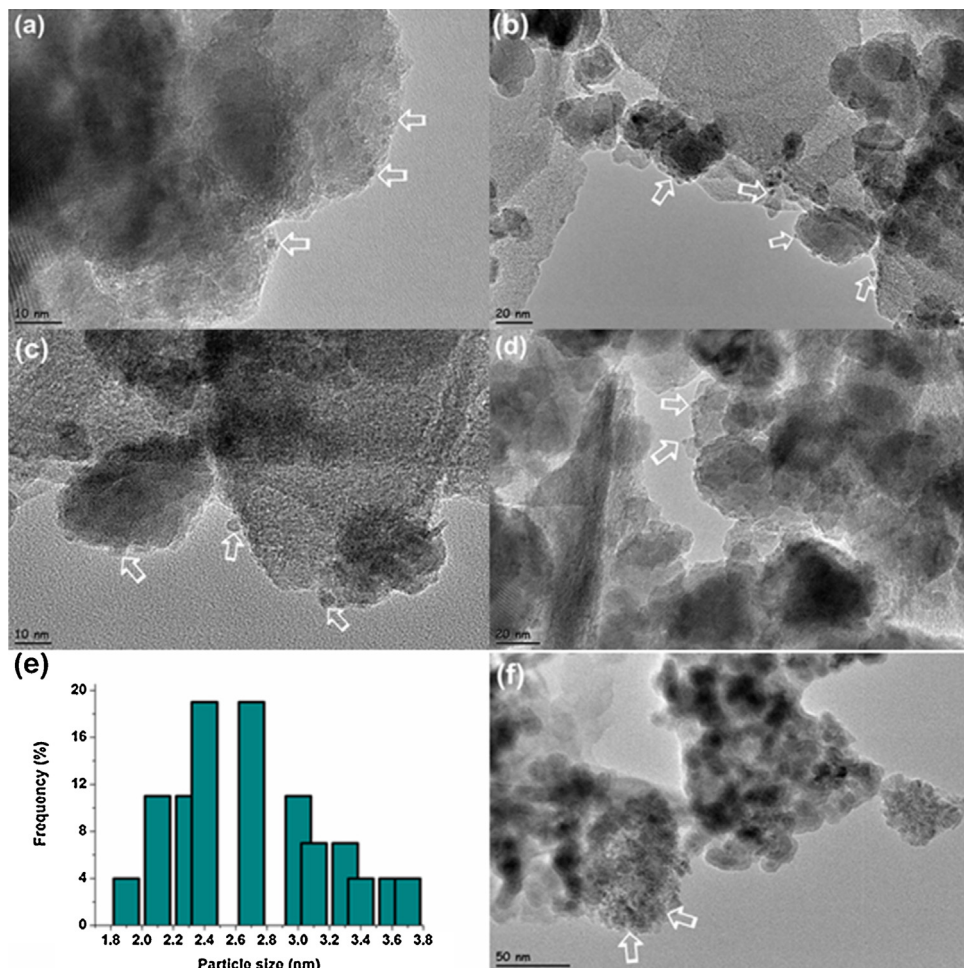


Fig. 12. (a-d) TEM images of $\text{Pd}^0/\text{CoFe}_2\text{O}_4$ (1.0 wt% Pd) at different magnifications (the arrows show the Pd NPs), (e) particle size distribution of $\text{Pd}^0/\text{CoFe}_2\text{O}_4$ (mean size = $2.74 \pm 0.49 \text{ nm}$), and (f) TEM image of $\text{Pd}^0/\text{CoFe}_2\text{O}_4$ after fifth use (the arrows show the aggregation of Pd NPs).

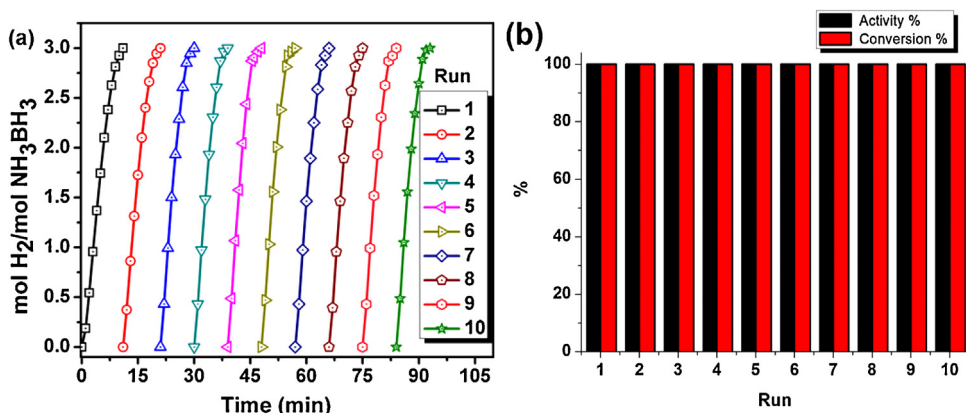


Fig. 13. (a) Plots of equivalent H_2 per mole of AB versus time in successive runs of catalytic hydrolysis of ammonia borane (0.10 M) starting with 50 mg of $\text{Pd}^0/\text{PDA-Fe}_2\text{O}_4$ catalyst (1.08 wt\% Pd) at $25.0 \pm 0.1^\circ\text{C}$ and (b) the corresponding percent initial catalytic activity and the percent conversion of AB for each run.

consuming but also causes significant loss of the catalytic material during the isolation process. Both problems can be avoided by using magnetically separable catalysts like the one in the present case (Fig. S3, see SI). $\text{Pd}^0/\text{CoFe}_2\text{O}_4$ and $\text{Pd}^0/\text{PDA–CoFe}_2\text{O}_4$ catalysts are magnetically separable, thus, can be recovered by an external magnet and used for several cycles of catalytic reaction. The reusability of $\text{Pd}^0/\text{CoFe}_2\text{O}_4$ and $\text{Pd}^0/\text{PDA–CoFe}_2\text{O}_4$ catalysts was easily tested in successive runs of hydrolysis by magnetically isolating the catalyst from the reaction solution after a previous run and redispersing it in a new batch of AB solution at $25.0 \pm 0.1^\circ\text{C}$. The catalytic activity of the supernatant solutions obtained by magnetic separation of the two samples after the first run of hydrolysis was also tested in the hydrolysis of AB (100 mM) under the same conditions and both supernatant solutions were found to be catalytically silent in the hydrolysis of AB. This observation indicates that there is no leaching of palladium nanoparticles into the solution during the hydrolysis and palladium(0) nanoparticles are kinetically competent catalysts in the hydrolysis of ammonia borane.

The results of reusability tests reveal that $\text{Pd}^0/\text{CoFe}_2\text{O}_4$ catalyst loses 10% of its initial catalytic activity after the fifth run (Fig. 11) though with 100% conversion of AB in all the cycles, i.e. releasing 3.0 equivalent H_2 per mole of AB. The deactivation is essentially due to the agglomeration of palladium(0) nanoparticles as seen from the TEM images taken after fifth run of hydrolysis reaction (Fig. 12f). On the other hand, $\text{Pd}^0/\text{PDA–CoFe}_2\text{O}_4$ catalyst preserves its initial catalytic activity in the subsequent runs of hydrolytic dehydrogenation of AB up to 10th run (Fig. 13) still providing 100% conversion in each run. Table 1 shows the comparison of palladium-based catalysts in terms of catalytic activity retained after multiple use in hydrolysis of ammonia borane. Magnetically isolable $\text{Pd}^0/\text{PDA–CoFe}_2\text{O}_4$ catalyst provides exceptionally reusable performance even after the tenth use as compared to the other palladium-based catalysts. The stability of the $\text{Pd}^0/\text{PDA–CoFe}_2\text{O}_4$ catalyst is due to the anchoring of the palladium(0) nanoparticles by the *N*- and *O*-binding sites of the polydopamine layers on the surface of CoFe_2O_4 .

All the results reveal that a controllable generation of pure hydrogen gas from the hydrolysis of ammonia borane can be achieved by using magnetically separable palladium(0) nanoparticles supported on polymer coated cobalt ferrite. By using this magnetically separable and reusable catalyst, hydrogen release can easily be controlled by changing the contact area of the catalyst to the ammonia borane solution. As the reactant and products of the hydrolysis reaction are stable and environmentally benign, the controllable and safe hydrogen generation from ammonia borane in the presence of the magnetically separable palladium catalyst can be used for the fuel cell applications at ambient temperature.

4. Conclusion

Palladium(0) nanoparticles supported on cobalt ferrite ($\text{Pd}^0/\text{CoFe}_2\text{O}_4$) are found to be highly active and magnetically isolable catalyst in hydrogen generation from the hydrolysis of AB providing a turnover frequency of 290 min^{-1} . However, the $\text{Pd}^0/\text{CoFe}_2\text{O}_4$ catalyst losses its activity slightly in successive runs of hydrolysis in reusability tests. Polydopamine coating of magnetic cobalt ferrite provides high reusability for the palladium catalyst. Polydopamine layer on the surface of cobalt ferrite particles has the capability to coordinate metal ions or atoms through the *N*- and *O*-binding sites on the surface of polymer layer. Thus, the palladium(II) ions can be impregnated and reduced on the surface of polymer coated cobalt ferrite to form palladium(0) nanoparticles anchored via coordinating to the polymer layer on the surface of CoFe_2O_4 powders. The resulting $\text{Pd}^0/\text{PDA–CoFe}_2\text{O}_4$ is also highly active catalyst providing a TOF value of 175 min^{-1}

in hydrogen generation from the hydrolysis of AB at $25.0 \pm 0.1^\circ\text{C}$. More importantly, the magnetically isolable $\text{Pd}^0/\text{PDA–CoFe}_2\text{O}_4$ catalyst is highly reusable and retains its initial catalytic activity even after 10th use in the hydrolysis of ammonia borane releasing 3 equivalent H_2 per mole of AB. The stability of the $\text{Pd}^0/\text{PDA–CoFe}_2\text{O}_4$ catalyst upon reusing shows that dopamine coating of CoFe_2O_4 powders play a crucial role in the catalytic stability of palladium(0) nanoparticles due to the presence of the *N*- and *O*-binding sites of polymer layer on the surface of cobalt ferrite. Easy preparation, high catalytic activity and excellent reusability performance of palladium(0) nanoparticles supported on polydopamine coated cobalt ferrite make $\text{Pd}^0/\text{PDA–CoFe}_2\text{O}_4$ a promising catalyst to be employed in developing highly efficient and portable hydrogen generation systems using ammonia borane for the fuel cell applications.

Acknowledgements

Partial support by Turkish Academy of Sciences is acknowledged. JM is thankful to Scientific and Technological Research Council of Turkey (TUBITAK) for the fellowship (Research Fellowship Program 2216 for International Researchers).

Appendix A. Supplementary data

Supplementary data associated with this article can be found, in the online version, at <http://dx.doi.org/10.1016/j.apcatb.2017.02.037>.

References

- [1] W.-W. Zhan, Q.-L. Zhu, Q. Xu, *ACS Catal.* 6 (2016) 6892–6905.
- [2] Q. Yao, Z.-H. Lu, W. Huang, X. Chen, J. Zhu, *J. Mater. Chem. A* 4 (2016) 8579–8583.
- [3] G. Moussa, R. Moury, U.B. Demirci, P. Miele, *Int. J. Hydrogen Energy* 38 (2013) 7888–7895.
- [4] M. Sasidharan, P. Bhanja, C. Senthila, A. Bhaumik, *RSC Adv.* 6 (2016) 11370–11377.
- [5] M.A. Khalily, H. Eren, S. Akbayrak, H.H. Susapto, N. Biyikli, S. Özkar, M.O. Guler, *Angew. Chem. Int. Ed.* 55 (2016) 12257–12261.
- [6] Y. Tonbul, S. Akbayrak, S. Özkar, *Int. J. Hydrogen Energy* 41 (2016) 11154–11162.
- [7] W.-d. Zhong, X.-k. Tian, C. Yang, Z.-x. Zhou, X.-w. Liu, Y. Li, *Int. J. Hydrogen Energy* 41 (2016) 15225–15235.
- [8] S. Akbayrak, Y. Tonbul, S. Özkar, *Dalton Trans.* 45 (2016) 10969–10978.
- [9] Q. Yao, W. Shi, G. Feng, Z.-H. Lu, X. Zhang, D. Tao, D. Kong, X. Chen, *J. Power Sources* 257 (2014) 293–299.
- [10] S. Akbayrak, Y. Tonbul, S. Özkar, *Appl. Catal. B* 198 (2016) 162–170.
- [11] T.J. Clark, G.R. Whittle, I. Manners, *Inorg. Chem.* 46 (2007) 7522–7527.
- [12] M. Urushizaki, H. Kitazawa, S. Takano, R. Takahata, S. Yamazoe, T. Tsukuda, *J. Phys. Chem. C* 119 (2015) 27483–27488.
- [13] K. Fuku, R. Hayashi, S. Takakura, T. Kamegawa, K. Mori, H. Yamashita, *Angew. Chem. Int. Ed.* 52 (2013) 7446–7450.
- [14] K. Aranishi, Q.-L. Zhu, Q. Xu, *ChemCatChem* 6 (2014) 1375–1379.
- [15] J.-M. Yan, X.-B. Zhang, H. Shioyama, Q. Xu, *J. Power Sources* 195 (2010) 1091–1094.
- [16] P.-Z. Li, A. Ajiaz, Q. Xu, *Angew. Chem. Int. Ed.* 51 (2012) 6753–6756.
- [17] Q. Xu, M. Chandra, *J. Power Sources* 163 (2006) 364–370.
- [18] J.-M. Yan, X.-B. Zhang, S. Han, H. Shioyama, Q. Xu, *Angew. Chem. Int. Ed.* 47 (2008) 2287–2289.
- [19] M. Dinç, Ö. Metin, S. Özkar, *Catal. Today* 183 (2012) 10–16.
- [20] M. Zahmakiran, S. Özkar, *Nanoscale* 3 (2011) 3462–3481.
- [21] R.B.N. Baig, R.S. Varma, *Chem. Commun.* 49 (2013) 752–770.
- [22] M. Chandra, Q. Xu, *J. Power Sources* 168 (2007) 135–142.
- [23] M. Rakap, *Appl. Catal. B* 163 (2015) 129–134.
- [24] S. Shylesh, V. Schünemann, W.R. Thiel, *Angew. Chem. Int. Ed.* 49 (2010) 3428–3459.
- [25] D. Wang, D. Astruc, *Chem. Rev.* 114 (2014) 6949–6985.
- [26] J.M. Liu, X.G. Peng, W. Sun, Y.W. Zhao, C.G. Xia, *Org. Lett.* 10 (2008) 3933–3936.
- [27] J. Jung, S. Bae, W. Lee, *Appl. Catal. B* 127 (2012) 148–158.
- [28] M.B. Gawande, P.S. Branco, R.S. Varma, *Chem. Soc. Rev.* 42 (2013) 3371–3393.
- [29] H. Zheng, J. Wang, S.E. Lofland, Z. Mohaddes-Ardabili, L. Ma, T. Zhao, L. Salamanca-Riba, S.R. Shinde, S.B. Ogale, F. Bai, D. Viehland, Y. Jia, D.G. Schlom, M. Wuttig, A. Roytburd, R. Ramesh, *Science* 303 (2004) 661–663.
- [30] S. Akbayrak, M. Kaya, M. Volkan, S. Özkar, *Appl. Catal. B: Environ.* 147 (2014) 387–393.

[31] S. Akbayrak, M. Kaya, M. Volkan, S. Özkar, *J. Mol. Catal. A: Chem.* 394 (2014) 253–261.

[32] J. Chen, Z.-H. Lu, Y. Wang, X. Chen, L. Zhang, *Int. J. Hydrogen Energy* 40 (2015) 4777–4785.

[33] M. Kaya, M. Zahmakiran, S. Özkar, M. Volkan, *ACS Appl. Mater. Interfaces* 4 (2012) 3866–3873.

[34] J. Manna, S. Akbayrak, S. Özkar, *RSC Adv.* 6 (2016) 102035–102042.

[35] V. Polshettiwar, R.S. Varma, *Org. Biomol. Chem.* 7 (2009) 37–40.

[36] C. Xu, K. Xu, H. Gu, R. Zheng, H. Liu, X. Zhang, Z. Guo, B. Xu, *J. Am. Chem. Soc.* 126 (2004) 9938–9939.

[37] C. Liu, A.J. Rondinone, Z.J. Zhang, *Pure Appl. Chem.* 72 (2000) 37–45.

[38] T. Prozorov, P. Palo, L. Wang, M. Nilsen-Hamilton, D. Jones, D. Orr, S.K. Mallapragada, B. Narasimhan, P.C. Canfield, Ruslan Prozorov, *ACS Nano* 1 (2007) 228–233.

[39] C.J. Jenks, S.-L. Chang, J.W. Anderegg, P.A. Thiel, D.W. Lynch, *Phys. Rev. B: Condens. Matter Mater. Phys.* 54 (1996) 6301–6306.

[40] M. Peuckert, *J. Phys. Chem.* 89 (12) (1985) 2481–2486.

[41] X. Han, L. Zhang, C. Li, *RSC Adv.* 4 (2014) 30536–30541.

[42] J. Liebscher, R. Mrówczyński, H.A. Scheid, C. Filip, N.D. Hădăde, R. Turcu, A. Bende, S. Beck, *Langmuir* 29 (2013) 10539–105448.

[43] S. Akbayrak, S. Özkar, *ACS Appl. Mater. Interfaces* 4 (2012) 6302–6310.

[44] A. Bruix, J.A. Rodriguez, P.J. Ramírez, S.D. Senanayake, J. Evans, J.B. Park, D. Stacchiola, P. Liu, J. Hrbek, F. Illas, *J. Am. Chem. Soc.* 134 (2012) 8968–8974.

[45] N. Acerbi, S.C. Edman Tsang, G. Jones, S. Golunski, P. Collier, *Angew. Chem. Int. Ed.* 52 (2013) 7737–7741.

[46] S.J. Tauster, S.C. Fung, R.L. Garten, *J. Am. Chem. Soc.* 100 (1978) 170–175.

[47] K. An, S. Alayoglu, N. Musselwhite, S. Plamthottam, G. Melaet, A.E. Lindeman, G.A. Somorjai, *J. Am. Chem. Soc.* 135 (2013) 16689–16696.

[48] P. Hu, Z. Huang, Z. Amghouz, M. Makkee, F. Xu, F. Kapteijn, A. Dikhtiarenko, Y. Chen, X. Gu, X. Tang, *Angew. Chem. Int. Ed.* 53 (2014) 3418–3421.

[49] J.C. Frost, *Nature* 334 (1988) 577–580.

[50] M. Chandra, Q. Xu, *J. Power Sources* 159 (2006) 855–860.

[51] M. Mahyari, A. Shaabani, *J. Mater. Chem. A* 2 (2014) 16652–16659.

[52] H. Dai, J. Su, K. Hu, W. Luo, G. Cheng, *Int. J. Hydrogen Energy* 39 (2014) 4947–4953.

[53] J. Wang, Y.-L. Qin, X. Liu, X.-B. Zhang, *J. Mater. Chem.* 22 (2012) 12468–12470.

[54] D. Sun, V. Mazumder, Ö. Metin, S. Sun, *ACS Nano* 5 (2011) 6458–6464.

[55] K. Güngörmez, Ö. Metin, *Appl. Catal. A* 494 (2015) 22–28.

[56] Ö. Metin, E. Kayhan, S. Özkar, J.J. Schneider, *Int. J. Hydrogen Energy* 37 (2012) 8161–8169.

[57] Y. Li, Y. Dai, X.-K. Tian, *Int. J. Hydrogen Energy* 40 (2015) 9235–9243.

[58] M. Rakap, S. Özkar, *Int. J. Hydrogen Energy* 36 (2011) 7019–7027.

[59] P. Xi, F. Chen, G. Xie, C. Ma, H. Liu, C. Shao, J. Wang, Z. Xu, X. Xu, Z. Zeng, *Nanoscale* 4 (2012) 5597–5601.

[60] B. Kılıç, S. Şençanlı, Ö. Metin, *J. Mol. Catal. A* 361–362 (2012) 104–110.

[61] M. Rakap, E.E. Kalu, S. Özkar, *Int. J. Hydrogen Energy* 36 (2011) 1448–1455.

[62] M. Rakap, S. Özkar, *Int. J. Hydrogen Energy* 35 (2010) 1305–1312.

[63] Ö. Metin, S. Sahin, S. Özkar, *Int. J. Hydrogen Energy* 34 (2009) 6304–6313.

[64] M. Chandra, Q. Xu, *J. Power Sources* 156 (2006) 190–194.